Investigating High N/O Blue Compact Galaxies with VLT-IFUs

Bethan James[1]
Yiannis Tsamis[2]
Jeremy Walsh[2]
Mike Barlow[3]
Mark Westmoquette[2]

[1] Institute of Astronomy, University of Cambridge, United Kingdom
[2] ESO
[3] Department of Physics and Astronomy, University College London, United Kingdom

A series of publications concerning the spatially resolved chemical abundance analyses of a sample of blue compact galaxies, using VLT–FLAMES and VLT–VIMOS integral field observations, is summarised. Four out of the five galaxies observed were previously labelled as having enhanced nitrogen-to-oxygen (N/O) ratios for their metallicities. However, our analyses reveal regions of enhanced N/O in only three of these galaxies. The integral field unit observations provide maps of the physical and chemical conditions within each system, along with maps of stellar population age, star-forming rate and emission from Wolf–Rayet stars. By combining this plethora of information, we have attempted to disentangle the relationship between N-enrichment and WR stars in blue compact galaxies, and reveal that it is far from being one to one.

High N/O ratio blue compact galaxies

Blue compact galaxies (BCGs) in the nearby Universe provide a means of studying chemical evolution and star formation processes in chemically unevolved environments. They typically have low masses and low metallicities (1/50–1/3 $Z_{\odot}$), making them attractive analogues to the young building-block galaxies thought to exist in the high-z primordial Universe (see Kunth & Ostlin [2000] for a review). Having experienced only low levels of star formation in the past, their present-day bursts of star formation occur in relatively pristine environments, and, as such, investigating their chemical evolution can impact our understanding of primordial galaxies and galaxy evolution in general.

One particularly puzzling aspect of galaxy chemical evolution is the nitrogen-to-oxygen ratio. Although most elements have a linear relationship with galaxy metallicity (here oxygen abundance is taken to represent metallicity in the absence of available stellar abundance indicators), nitrogen shows a more complex dependence (Izotov & Thuan, 1999; Izotov et al., 2006; and references therein). At low metallicities, nitrogen behaves as a primary-production element and at high metallicities it behaves as a secondary-production element. At intermediate metallicities, however, there is a large scatter, with a subset of galaxies showing N/O ratios up to three times higher than expected for their metallicity. The most popular explanation for this nitrogen overabundance is chemical pollution from the nitrogen-rich winds of Wolf–Rayet (WR) stars, a theory based primarily on the simultaneous detection of WR emission and high N/O ratios from long-slit spectroscopic observations (Pustilnik et al., 2004; Brinchmann et al., 2008). Whilst this was certainly found to be the case in NGC 5253 (Monreal-Ibero et al., 2012; and references therein), spatially resolved abundance studies are showing that this relationship is not as clear cut as once thought.

With the aim of understanding this scatter, we have used integral field unit (IFU) spectroscopy to observe a sample of BCGs for which previous studies reported anomalously high N/O ratios. We also observed one control object within our sample (UM462), which had a reported normal N/O ratio for its metallicity. IFU data afforded us the spatial information needed to relate the chemical properties to the physical, kinematical and stellar properties of each galaxy. The sample consisted of Mrk996 (James et al., 2009), UM462 and UM420 (James et al., 2010), UM448 (James et al., 2012) and Haro11 (James et al., 2013). Images of Mrk996, UM448 and Haro11 are shown in Figure 1, with the IFU apertures overlaid.

Mapping the complex emission profiles

Two IFUs were used for this sample in order to match the extent of the emission regions to the IFU size: VLT–VIMOS (used to observe Mrk996, UM420 and UM462) and VLT–FLAMES/Argus (used to observe Haro11 and UM448). VIMOS observations were taken using the HRblue and HRorange settings, covering a total wavelength range of 415–740 nm, while FLAMES observations were taken in the LR1–3 and LR6 modes, covering 362–508 nm and 644–718 nm. The observations were designed to cover all of the important emission lines needed to perform a chemical abundance analysis, as detailed below. The data were reduced using standard reduction pipelines, converted into (x, y and wavelength) datacubes and corrected for differential atmospheric refraction.

Upon inspection of the datacubes, it was apparent that the majority of the sample (all except UM420 and UM462) displayed complex emission line profiles at the observed spectral resolution, so that each line was made up of multiple components (see an example in Figure 2 for Haro11). This indicated that along each spatially resolved sightline, there is emission from gas with different physical properties, e.g., velocity, turbulence, temperature and/or density. It was therefore necessary, and indeed useful, to decompose the line profiles and perform a separate chemical abundance analysis on each velocity component, thus undertaking a chemodynamical approach.

We used an automated line-fitting routine to fit the emission components throughout each datacube, aided by a likelihood ratio method (Westmoquette et al. 2001) to rigorously determine the optimum number of Gaussians required to fit each observed profile. Once the emission was deconvolved into its separate components (typically a narrow component; a broad component underlying the narrow one; and sometimes a third, weaker and kinematically offset component), we created flux, velocity and line-width maps for each of the separate components.

Mapping the de-convolved line profiles and creating separate kinematical maps for each component, provided insight into the complex motions of the gas within these irregular systems. Although the kinematics of the narrow-component emitting gas showed signs of ordered, solid-body rotation (in UM448 and

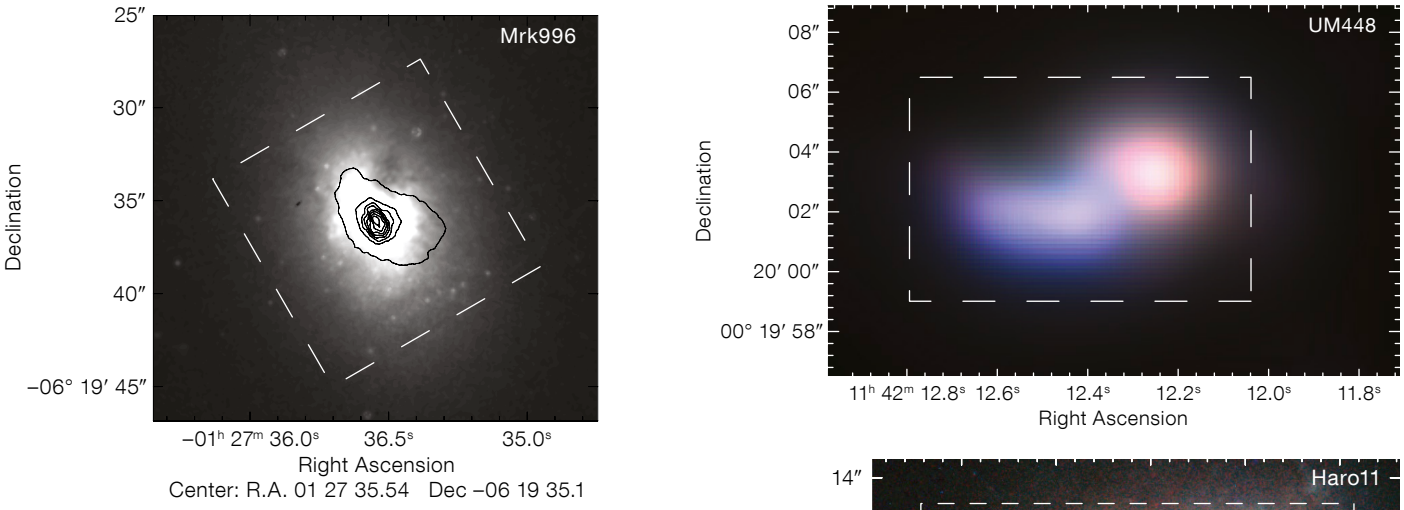

Figure 1. Three of the five BCGs observed within our sample, with the respective IFU aperture overlaid (dashed line). Clockwise from left: Mrk996 (HST F569W WFPC2 image with VLT-VIMOS aperture); UM448 (SuSI2 *RVB*-band composite image, VLT-FLAMES aperture); Haro11 (HST-ACS F220W, F330W and F814W colour composite, VLT-FLAMES aperture). North is up and east is left in all images.

Figure 2. An example of a complex emission-line profile as seen throughout our sample of blue compact galaxies, and the flux maps created by deconvolving its velocity components. The top row shows an example three-component Hα line profile seen in Haro11. The highlighted component (red line) indicates to which component the maps below correspond.

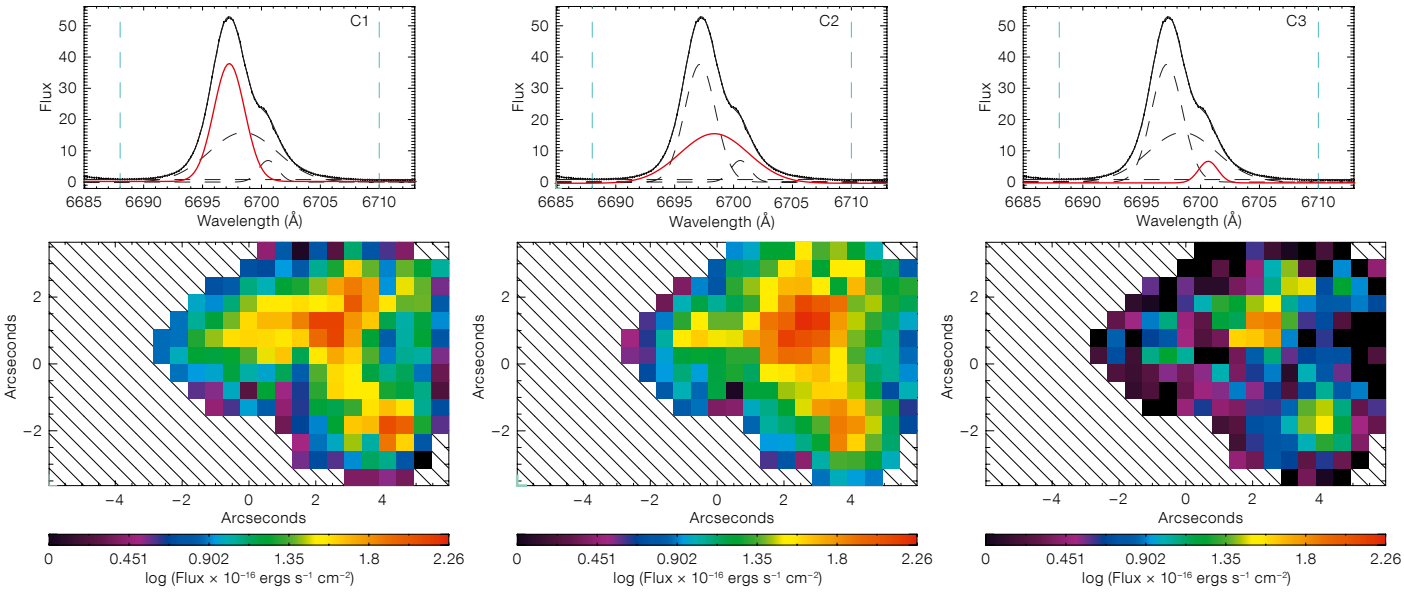

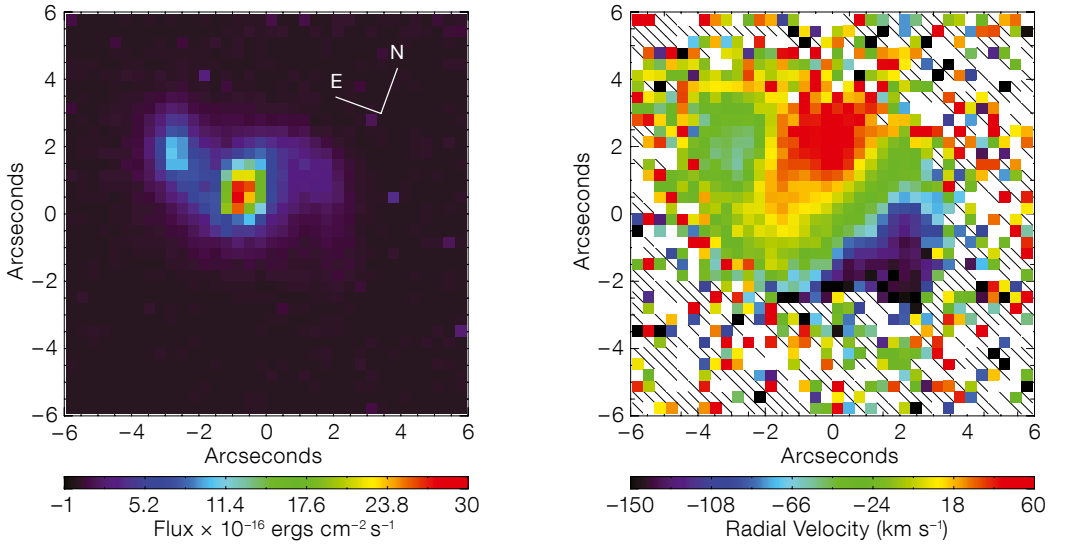

Figure 3. A merger in process where the radial velocity maps reveal the complex dynamical state of a galaxy. The left-hand panel shows UM420 in Hα whose morphology is suggestive of a spiral-type structure. However, the radial velocity map on the right reveals that the galaxy is in fact made up of two kinematically distinct bodies probably in the process of merging: one smaller body in the east and a larger central body.

Mrk996), the broad component emission was often offset from this. For example, in Mrk996 we detected the kinematic signature of a turbulent two-arm spiral structure within the nucleus, while in UM420 (Figure 3) and UM448 clear signs of a merger between two distinct kinematical bodies are seen. In Haro11, the gas volume emitting the broad velocity profile is rotating in an orthogonal direction to that of the narrow-component emitting gas — revealing a counter-rotating disc of turbulent gas within the central knot of star formation.

In order to derive accurate chemical abundances, we used the "direct method", which is based on direct measurements of the electron temperature and density of the emitting nebulosity. Abundance maps were derived from reddening-corrected line intensity maps, an electron temperature map (calculated from [O III] (λ5007 + λ4959)/λ4363 line ratios, as shown in Figure 4) and an electron density map (calculated from [S II] λ6716/λ6731 ratios). In this way, each spatial pixel (or spaxel) has its own unique set of measured physical conditions from which to derive the gas chemical composition. Ionic nitrogen, oxygen, sulphur and neon abundances were converted into elemental abundances relative to hydrogen using off-the-shelf ionisation correction factors (ICF; a fairly robust approach in H II region research as the ICFs have been benchmarked against nebular models). Chemical abundances were also calculated using spectra integrated over individual star-forming regions and also the galaxy as a whole.

Several properties were mapped throughout each galaxy, including star formation rate (derived from the Hα flux), the age of the ionising stellar population (from the equivalent width of Hβ), and maps of the WR stellar population. The latter were created from the Wolf–Rayet spectral signature at 465.0 nm (the blue bump). When combined with the chemical abundance maps, the spatial distribution of these properties was used to help disentangle the chemical evolutionary stage and/or chemical feedback processes occurring within each galaxy.

An insight into N-enrichment and its origins

From our IFU sample of four pre-selected high-N/O galaxies, we found that three scenarios were at play:

1) Misdiagnosed high-N/O status: UM420

UM420 was previously thought, based on long-slit studies, to have an N/O ratio 0.5 dex higher than expected for its metallicity. Following the spatially resolved analysis with VIMOS, enhanced N/O was not found to be the case for either of its two main star-forming regions and across the whole galaxy. UM420 shows minimal nitrogen or oxygen abundance variations throughout, implying that this galaxy has not been caught in the wake of any major chemical self-enrichment episode, and has an oxygen abundance of one-third solar.

In fact, a difference between abundances derived from spectra integrated over the entire galaxy and those derived from regional averages across the abundance maps, was found throughout our studies. Interestingly, abundance ratios relative to hydrogen were found to be inconsistent, whereas those relative to oxygen were in agreement within the uncertainties. This is possibly due to the former having a higher dependency on electron temperature that can be erroneously calculated when using ratios from summed spectra, as they tend to suffer from luminosity weighting. This effect can have significant consequences for abundance measurements based on integrated spectra of high-redshift galaxies.

2) High N/O ratio in the presence of numerous WR stars: Mrk996

The case of Mrk996 was most intriguing. Although the majority of the emission lines showed both broad and narrow component emission (as reported by Thuan, Izotov & Lipovetsky, 1996), certain lines are only detected in their broad-component form — namely the temperature-sensitive lines ([N II] 575.5 nm and [O III] 436.3 nm), which are only emitted from the very core of the galaxy (see Figure 5). A separate analysis of the broad

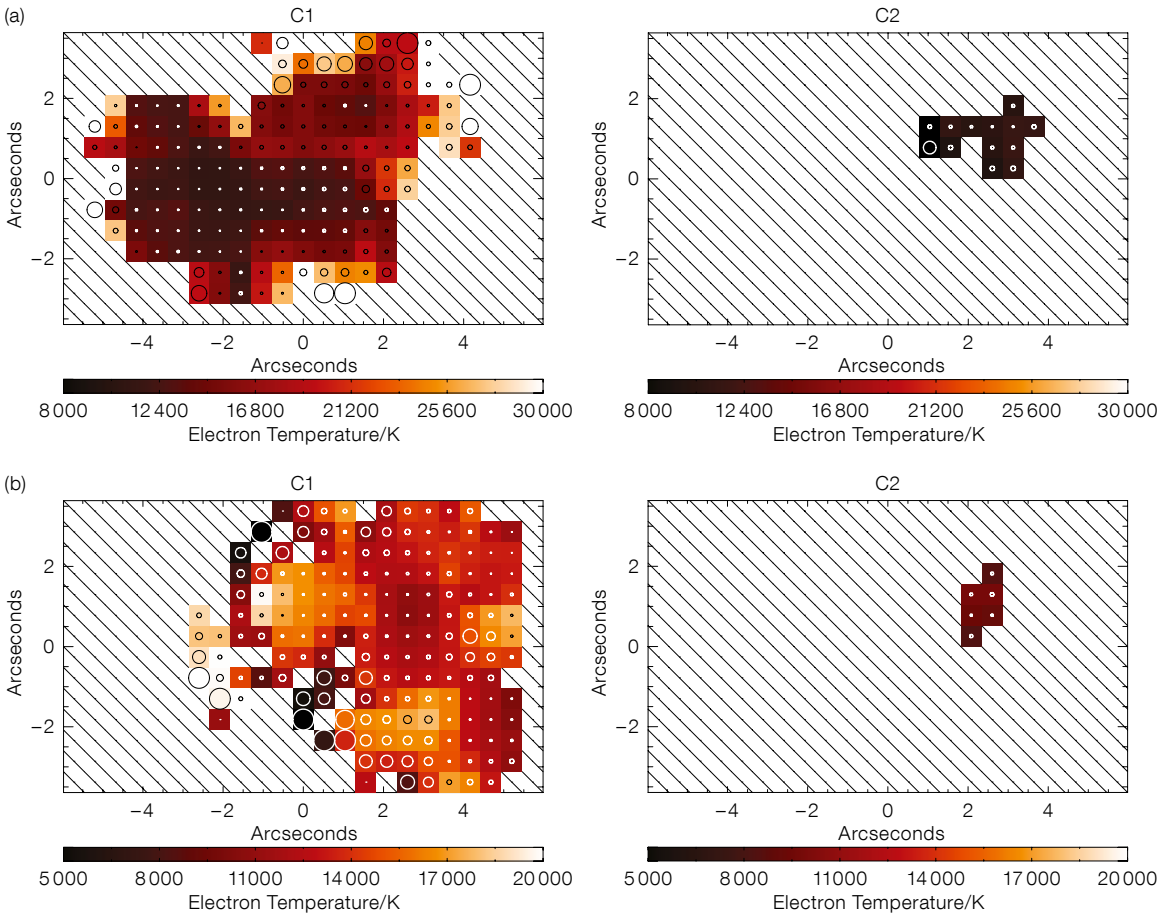

Figure 4. Electron temperature maps of (a) UM448 and (b) Haro11. The circles overlaid represent the size of the uncertainties within each spaxel's electron temperature. These maps were used in conjunction with electron density maps to derive chemical abundance maps, ensuring that each spaxel in the flux maps had its own set of physical conditions from which to derive its chemical abundance. C1 refers to the narrow, strong, emission component whereas C2 refers to the broad, underlying emission component.

and narrow components detected by VIMOS has helped to isolate the previously reported N-enrichment to the broad-component gas in the galaxy's nucleus. The abundance of nitrogen there is found to be 20 times higher than in the surrounding narrow-line region. No other element shows a pronounced difference in abundance between the two gas components.

The blue WR feature summed over the galaxy indicates the presence of approximately 2600 WNL (late WR-type with enhanced N) stars and 400 WC (WR-type with enhanced C) stars within the turbulent nuclear region (Figure 5). The equivalent width of Hβ indicates a stellar age of 4.5 Myr in this region — an age sufficiently old to have allowed massive stars in the galaxy to evolve to the WR stage. Together, these pieces of information indicate that the overabundance of nitrogen in the broad-component emission can be attributed to the cumulative effect of N-enriched winds of WR stars.

In addition, the N-enhanced material is spatially coincident with a region of extremely high electron density (~ 10^7 cm^{-3}, compared to typical H II region densities of ~ 100 cm^{-3}), which may have impeded and pressurised the WR winds, allowing their metal-rich ejecta to mix with the cooler phases and subsequently become observable.

At present, only one other dwarf starburst galaxy has been reported to display localised N-enrichment, NGC 5253. Deep VLT spectroscopy by Lopez-Sanchez et al. (2007) of this well-studied galaxy showed increased N/O ratio in the two central starburst regions, and within one region the increase was isolated to the broad component only.

3) Perturbed BCGs with or without WR stars: UM448 & Haro11

UM448: The NTT SuSI2 image of UM448 shown in Figure 1 reveals that this galaxy is made up of two distinct stellar populations; an older, red population in the west and a younger, blue population towards the east. We observed this interacting system with FLAMES/Argus. An analysis of the global kinematics shows solid-body rotation aligned along the intersection of the two distinguished stellar regions, suggesting that they are in the process of merging. Whilst the N/O abundance ratio was found to be rather typical throughout UM448, there was a region of increased N/O located at the intercept of the two regions (Figure 6). Little or no WR-emission was detected throughout the galaxy, in spectra summed regionally or across the galaxy as a whole.

The region of enhanced N/O is, however, spatially coincident with a region of lower O/H. Judging from the kinematical maps, and ages of the stellar populations, we propose that the decrease in oxygen abundance is due to global processes occurring within the galaxy,

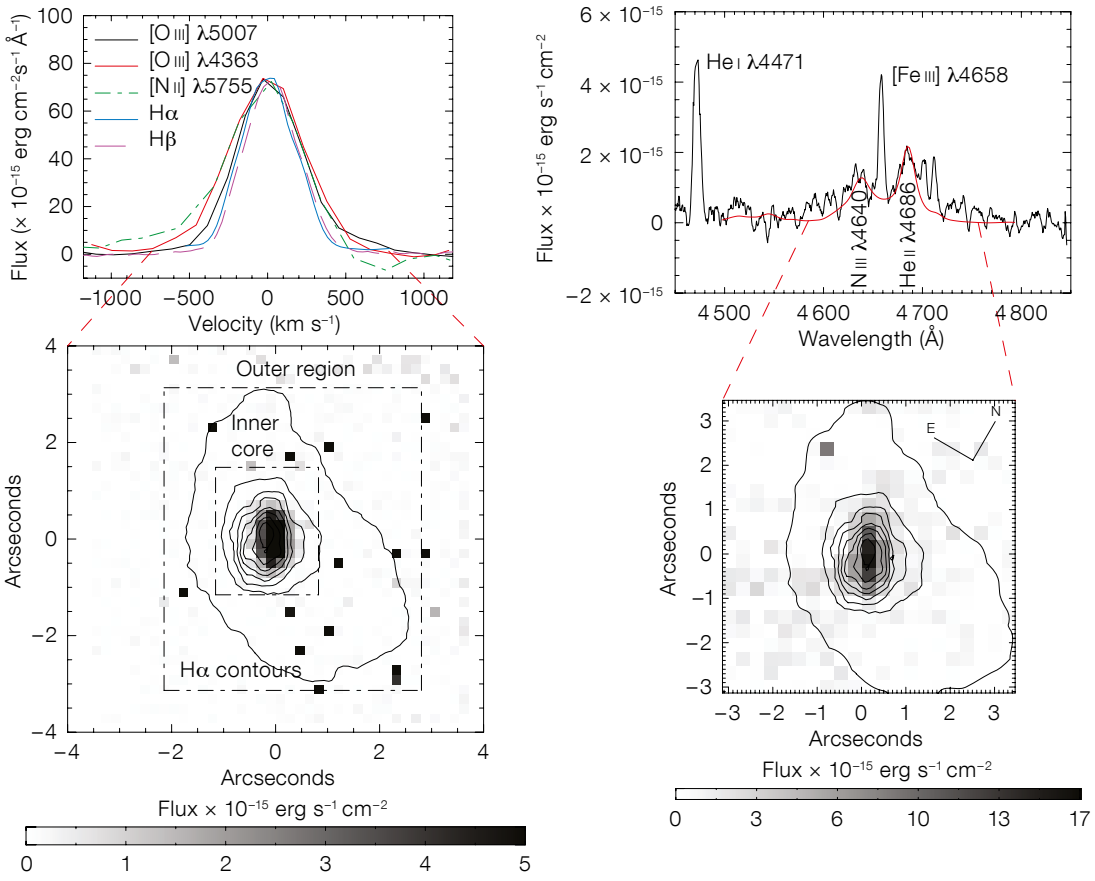

Figure 5. Left panel: Broad component profiles of five emission lines observed within Mrk996. The map shown below is the [O III] λ4363 flux map, displaying emission exclusively within the inner core of the galaxy. A high N/O ratio (5 × solar) was measured exclusively in the broad-component emission. Right panel: The blue bump at 465.0 nm, an emission feature attributable to ~ 2600 N-rich Wolf–Rayet stars and the emission map created from this feature is shown below. Comparing the flux maps, the spatial coincidence of WR-stars and broad-component emission, suggests that N-enrichment could be due to the N-rich winds of WR stars.

namely the likely interaction and/or merger between two bodies as inferred from the SuSI2 images and radial velocity maps, resulting in the accretion of metal-poor gas. This resonates with studies showing that interacting galaxies fall > 0.2 dex below the mass–metallicity relation of normal galaxies due to tidally induced large-scale inflow of metal-poor gas towards the central regions (e.g., Peeples et al., 2009).

Haro11: This galaxy is well known as being a local analogue to the high-redshift Lyman break galaxies. It has been studied in detail from X-ray to infrared wavelengths, being in a rare class of Lyman-α and Lyman-continuum emitters (James et al. [2013] and references therein). As can be seen in Figure 1, Haro11 consists of three distinct knots of emission that are kinematically connected. The galaxy displays complex emission profiles throughout the knots (see Figure 2). The eastern knot (called Knot C) is found to have a higher temperature (by ~ 4000 K) and consequently, an oxygen abundance that is 0.4 dex lower than the neighbouring regions. A region of enhanced N/O ratio is found specifically in Knot C, confirming previous studies that found an anomalously high N/O ratio in this system (Izotov & Thuan, 1999). However, maps of the WR emission throughout Haro11 reveal large WR populations (~ 900–1500 stars) in Knots A and B only.

Unlike UM448, the properties of Knot C are consistent with the mass–metallicity relationship at low galaxy masses, suggesting that the accretion of metal-poor gas is unlikely. Conversely, there may have been an outflow of oxygen-enriched gas due to supernovae (SNe). Further insight into the source's evolutionary stage was provided by the maps of stellar population age, which show that Knot C is 2–3 Myr older than Knots A and B (~ 4–5 Myr) and so it may indeed have experienced more SNe explosions than the younger knots. Alternatively, its age implies that its WR phase has recently been completed. This suggests that Knot C has had sufficient time to maximise the injection of nitrogen into the local interstellar medium (ISM) during the WR phase, which may still be relatively undiluted by subsequent mass-loss of lower mass stars. This case is further supported by Knot C having a lower current star formation rate (~ 0.09 $M_{\odot}$/year) as derived from its integrated Hα flux. Overall, it is clear that Knot C has undergone a separate evolutionary path to the other constituents of the galaxy.

In the younger Knots A and B, on the other hand, we observe the opposite scenario — normal N/O ratios and substantial WR populations (Figure 6). This suggests that we are catching the galaxy at an interesting point in its evolutionary path. We may be observing regions whose stars are in the process of expelling their processed nitrogen (which begins at ~ 5 Myr) and have not had enough time to be diluted by the ambient interstellar medium. If we take into consideration that the cooling and mixing of expelled material can last between 2–8 Myr over regions just 50 pc

in size, and that injection of material can begin as early as 2.5 Myr in the knot's evolution, it is unlikely that just 2 Myr later we would be able to observe the N-rich ejecta from the WR stars within regions as large as Knots A and B (0.4 and 1 kpc^2, respectively).

A complicated relationship

In our quest to understand the high N/O ratios found in a subset of blue compact galaxies, we have discovered that the measured N/O ratio can be sensitive to the type of spectroscopic technique used. Long-slit data can result in flux-weighted, and therefore misleading, line ratios when integrated over large spatial scales. For example, in the case of UM420, previous long-slit spectroscopy found that it had N/O levels 0.5 dex higher than other galaxies of a similar metallicity, whilst our spatially resolved analysis with VIMOS does not find any nitrogen excess.

In support of this result, for both Haro11 and UM448, we find that chemical abundances derived from spectra summed over the entire IFU aperture can differ significantly from those measured on resolved abundance maps. Therefore, although spatially resolved observations have the ability to detect temperature and abundance variations, thus isolating potential sites of enrichment, analyses based on integrated 1D spectra can introduce strong biases if a mixture of regions with different ionisation conditions and metal content are involved. Naturally, such effects could be potentially more severe for unresolved systems such as high redshift galaxies. Moreover, as the case of Mrk996 has clearly shown, accurate deconvolution of the line profiles with sufficiently high spectral resolution is at least as important: completely erroneous physical properties can otherwise be deduced.

Secondly, the spatial profile of the N/O ratio is highly dependent on the evolutionary stage of the galaxy and on environmental effects. In the three cases where spatial variations of the N/O ratio are detected (Mrk996, UM448 and Haro11), the mechanisms responsible are likely different. In Mrk996 we see

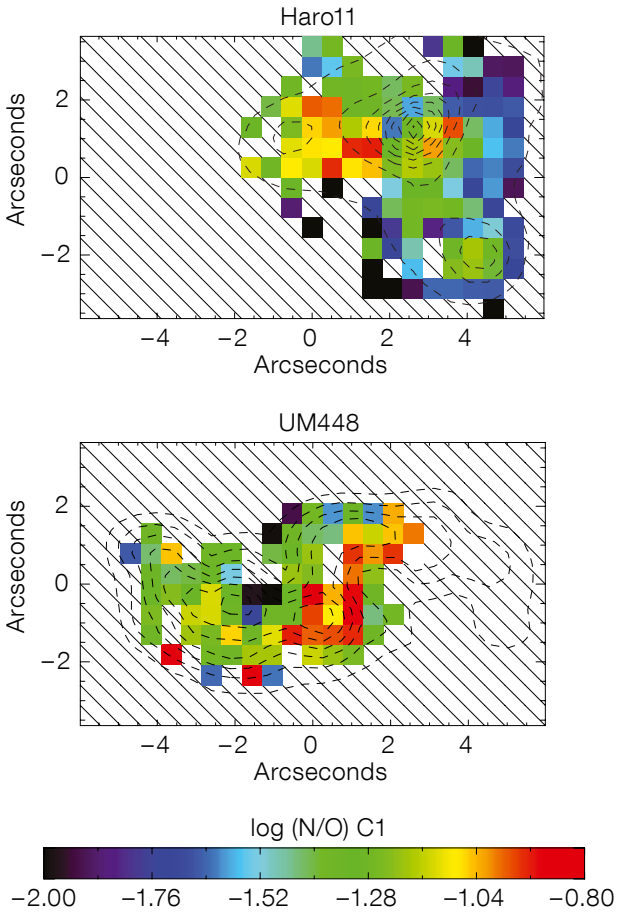

Figure 6. By performing a spatially resolved abundance analysis, we have been able to highlight regions of chemical enrichment. The figure shows maps of log(N/O) for Haro11 (upper panel) and UM448 (lower panel), for their narrow emission line components. A peak in N/O is seen in Haro11 in its most eastern knot, Knot C, whereas UM448 shows an increase in N/O towards the south. These maps, in conjunction with maps of WR emission, stellar population age, radial velocity and star formation rate, were used to investigate the mechanisms responsible for their heightened levels of N/O.

N-enrichment in the broad-component emission, originating in turbulent layers created by N-rich winds of numerous WR stars and confined within a very dense ISM in the centre of the galaxy. In UM448, the region of high N/O appears devoid of WR stars and the measured effect is likely due to accretion of metal-poor gas at the intercept of two merging bodies. Finally, in Haro11, we detect higher values of the N/O ratio in an older region where the WR phase has recently finished, whereas two younger regions that contain WR stars do not show enrichment signatures yet. From these three cases, it is clear that the relationship between localised N-enrichment and the existence of WR stars is far from being one to one. Instead, it is becoming apparent that the simultaneous detection of both WR features and enhanced N/O is a function of starburst age and the properties of the surrounding medium.

The VLT IFU observations that enabled these chemodynamical case studies reveal the complex kinematic and chemical properties of blue compact galaxies. A better understanding of the evolution of these systems can be achieved by IFU-driven analyses combined with chemical evolution models; this is the subject of ongoing work.

References

Brinchmann, J., Kunth, D. & Durret, F. 2008, A&A, 485, 657
Izotov, Y. I. & Thuan, T. X. 1999, ApJ, 511, 639
Kunth, D. & Ostlin, G. 2000, A&AR, 10, 1
Monreal-Ibero, A., Walsh, J. R. & Vílchez, J. M. 2012, A&A, 544, A60
James, B. L. et al. 2009, MNRAS, 398, 2
James, B. L., Tsamis, Y. G. & Barlow, M. J. 2010, MNRAS, 401, 759
James, B. L. et al. 2013, MNRAS, 428, 86
James, B. L. et al. 2013, MNRAS, 430, 2097
Lopez-Sanchez, A. R. et al. 2007, ApJ, 656, 168
Peeples, M. S., Pogge, R. W. & Stanek, K. Z. 2009, ApJ, 695, 259
Pustilnik, S. et al. 2004, A&A, 419, 469
Thuan, T. X., Izotov, Y. I. & Lipovetsky, V. A. 1996, ApJ, 463, 120
Westmoquette, M. S., Smith, L. J., Gallagher, J. S. 2011, MNRAS, 414, 3719